Exclusive Photothermal Heat Generation by a Gadolinium Bis(naphthalocyanine) Complex and Inclusion into Modified High-Density Lipoprotein Nanocarriers for Therapeutic Applications

Simon Mathew,[†,⊥] Tatsuya Murakami,[†,*] Hirotaka Nakatsuji,[‡] Haruki Okamoto,[‡] Nobuhiro Morone,[†] John E. Heuser,[†] Mitsuru Hashida,[†,§] and Hiroshi Imahori[†,‡,*]

[†]Institute for Integrated Cell-Material Sciences (WPI-iCeMS), Kyoto University, Sakyo-ku, Kyoto 606-8501, Japan, [‡]Department of Molecular Engineering, Graduate School of Engineering, Kyoto University, Nishikyo-ku, Kyoto 615-8510, Japan, and [§]Department of Drug Delivery Research, Graduate School of Pharmaceutical Sciences, Kyoto University, Sakyo-ku, Kyoto 606-8501, Japan. [⊥]Present address: Lab for Photonics and Interfaces, Institute of Chemical Sciences and Engineering, École Polytechnique Fédérale de Lausanne, Lausanne 1015, Switzerland.

ABSTRACT A hydrophobic gadolinium bis(naphthalocyanine) sandwich complex (GdSand) possessing several absorbances across visible and infrared wavelengths (up to 2500 nm) was solubilized in aqueous solution by uptake into a nascent mutant high-density lipoprotein (HDL) nanocarrier. The HDL nanocarrier was additionally functionalized with a trans-activator of transcription peptide sequence to promote efficient cell penetration of the drug delivery system (cpHDL). The dye-loaded nanocarrier (GdSand@cpHDL) exhibited photothermal heat generation properties upon irradiation with near-infrared (NIR) laser light, with controllable heat generation abilities as a function of the incident laser light power. Comparison of the photothermal behavior of the dyes GdSand and the well-explored molecular photothermal agent indocyanine green (ICG) in the cpHDL nanocarrier (*i.e.*, ICG@cpHDL) revealed two significant advantages of GdSand@cpHDL: (1) the ability to maintain elevated temperatures upon light absorption for extended periods of time, with a reduced degree of self-destruction of the dye, and (2) exclusive photothermal heat generation with no detectable singlet oxygen production leading to improved integrity of the cpHDL nanocarrier after irradiation. Finally, GdSand@cpHDL was successfully subjected to an *in vitro* study against NCI-H460 human lung cancer cells, demonstrating the proof-of-principle utility of lanthanide sandwich complexes in photothermal therapeutic applications.

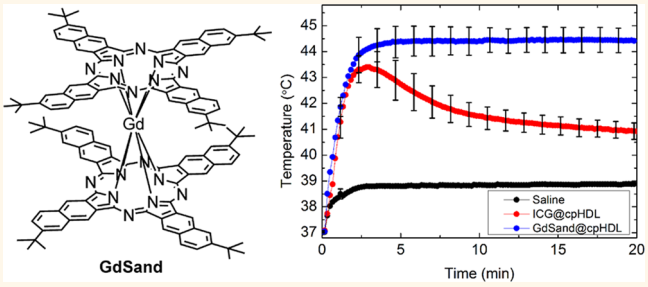

KEYWORDS: photothermal · hyperthermia · naphthalocyanine · high-density lipoprotein · drug delivery · phototherapy

Photothermal therapy (PTT) can be defined as achieving a positive therapeutic outcome by a light-induced temperature change within an organism. Photothermally active substances used for therapeutic purposes rely on the vibrational relaxation of a material after light absorption, thereby heating the surrounding medium.[1] PTT can be a highly targeted and site-specific treatment for solid tumors by combining directed heat generation through laser light irradiation and passive targeting through exploiting the enhanced permeability and retention (EPR) effect.[2,3] The overall photoinduced temperature change in PTT defines the photothermal mode of action, which can be classified as ablative or hyperthermic.[4,5] Photothermal ablation is where intense heat generation results in the necrosis of tissue. The mode of action for the ablative pathway can be either coagulative (50−99 °C) or evaporative

* Address correspondence to imahori@scl.kyoto-u.ac.jp, murakami@icems.kyoto-u.ac.jp.

Received for review July 3, 2013 and accepted September 20, 2013.

Published online September 20, 2013
10.1021/nn403384k

(>100 °C), resulting in the respective necrosis and/or carbonization of the tissue. Carbonization is an undesirable outcome, resulting in visible scarring of healed tissue and delayed healing time. Therefore, laser exposure should be carefully controlled to effect irreversible damage in a desired manner.[4−6] Alternatively, light-induced hyperthermia relies on smaller temperature increases (42−49 °C) sustained for greater periods of time (tens of minutes) to effect irreversible damage to the irradiated cells through the denaturation of proteins, enzymes, and disruption of cellular membranes.[5,7−11] Irrespective of the therapeutic mode of action (*i.e.*, ablative or hyperthermic), the fundamental molecular-design feature that photothermal agents possess is absorption in the infrared region of the spectrum. Specifically, absorption in the "therapeutic window" (between 750 and 900 nm) is essential in promoting efficient transmission of light to the deepest possible tissue depths.[12]

Achieving photothermally ablative properties is commonly conducted through the use of metal, especially gold, nanostructures.[13−25] Alternatively, the use of organic molecular agents such as indocyanine green,[26−30] carbon-based nanotubes,[31] fullerene,[32] graphene,[33] and macromolecular constructs[3,34−37] still prevails in the recent literature, demonstrating that strategies toward achieving hyperthermic abilities for PTT are attracting greater interest in the field of nanomedicine.

Nanoparticulate drug delivery systems (DDS) are commonly utilized to promote the passive localization of therapeutic agents at tumor sites by exploitation of the EPR effect.[3] Nanocarriers are especially useful for phototherapeutic dyes, as they are usually highly conjugated, planar, and lipophilic molecules, rendering them insoluble in aqueous systems.[38] The utilization of a DDS can prove invaluable in both maximizing the available drug and targeting the delivery of the drug to the desired site, with this strategy being actively exploited in the literature.

In the present study, we demonstrate the proof-of-principle ability of the gadolinium bis(naphthalocyanine) sandwich complex (GdSand, Figure 1) as a molecular sensitizer for hyperthermic photothermal applications. Compounds of this type have attracted interest from chemists and materials scientists because of their electrochromic and liquid-crystalline properties.[39−41] Applications of these sandwich complexes include color displays, gas sensors, resistors, field-effect transistors, nonlinear optical (NLO) materials, field-effect transistors (FETs), liquid-crystal semiconductors, and iono-electronic components.[40−43] We explored the potential of GdSand as a photothermal therapeutic because of unique and desirable qualities exhibited by this molecule:

1. Multiple absorptions across the visible and NIR region of the spectrum featuring an intense absorption maximum within the therapeutic window
2. The sandwich structure, facilitated by coordination of the rare-earth metal between two aromatic macrocycles, creating more absorptions in the middle infrared region, thus providing a greater range of light beyond that of a typical naphthalocyanine available for photothermal applications
3. The inhibition of singlet oxygen generation ($^1O_2$) due to light absorption beyond 1270 nm, promoting an exclusively photothermal mode of action regardless of the wavelength of light absorbed (*i.e.*, 770 nm utilized in this work), resulting in greater photostability of the sensitizer and nanocarrier

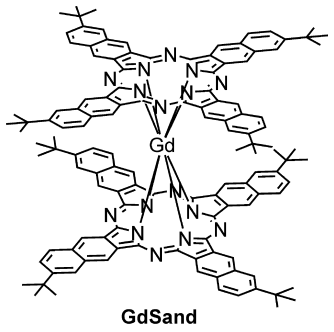

Figure 1. Structure of GdSand.[39]

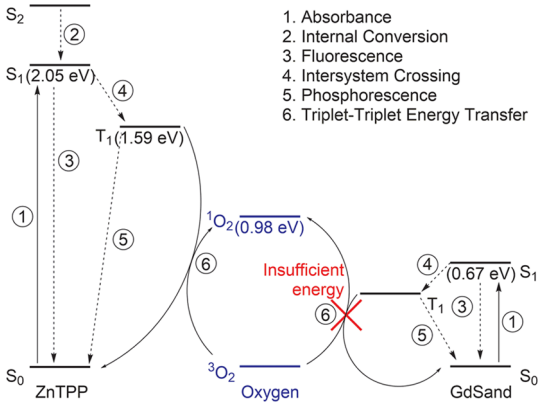

Figure 2. Modified Jablonski diagram of the production of singlet oxygen by zinc tetraphenylporphyrin (ZnTPP, representative of a phototherapeutic dye) and GdSand (optical band gap of GdSand calculated from the absorption peak at λ = 1854 nm (0.67 eV) from Figure 3).

The inhibition of singlet oxygen generation was hypothesized, as the presence of an extremely low energy absorption (out to 2500 nm) can result only in emission of energy exclusively beyond this wavelength. The ability to generate heat exclusively (and not $^1O_2$) upon irradiation is an attractive feature, as it provides an avenue toward greater stability of the dye and nanocarrier in the DDS. The energy requirement for $^1O_2$ generation is summarized in the modified Jablonski diagram (Figure 2). The GdSand sensitizer

possesses a lowest energy absorption (*vide infra*) at 1854 nm (0.67 eV), with the excited singlet state (S_1) experiencing a rapid intersystem crossing to generate the lower excited triplet state due to the heavy metal effect of gadolinium. Thus in accordance with Kasha's rule GdSand does not possess sufficient energy (1270 nm, 0.98 eV for $^1O_2$) to sensitize ground-state triplet oxygen, regardless of the wavelength of light utilized, to the highly reactive $^1O_2$ by an uphill energy transfer. The energetics of the GdSand sandwich complex is unique compared to the majority of naphthalocyanine dyes used in phototherapeutic applications, as traditional naphthalocyanine possesses a maximum wavelength between 700 and 850 nm, resulting in a photodynamical (*i.e.*, photodynamic therapy, PDT) mode of action through the generation of $^1O_2$ upon absorption of light.[44−48]

Although GdSand possessed distinct qualities that make it a potentially useful PTT agent, it did not exhibit appreciable solubility in aqueous solvents. Furthermore, as it is a molecular agent, it does not possess appreciable size to exploit the EPR effect. Therefore in this work, we explored the PTT ability of GdSand in a nanocarrier for the first time, to enable passive targeting to tumor sites. Passive targeting by the EPR effect promotes localization about a tumor site but does not guarantee cell internalization of the DDS. To ensure maximum efficacy of the DDS, the nanocarrier should possess functionality to promote cell internalization. Such functionality can be incorporated *via* the transactivating transcriptional activator (TAT) peptide motif.[49−52] The TAT peptide motif (YGRKKRRQRRR) is derived from HIV and is a class of cell-penetrating peptides (CPP) rich in the positively charged amino acids, enabling effective cell penetration through endocytosis.[53,54] In addition, cationic nanoparticles are reported to target tumor endothelial cells and exhibit enhanced vascular permeability.[55,56] In this study, we seek to assess the utility of the previously reported TAT peptide-fused nascent-HDL mutant (cpHDL) as a drug delivery device, as it has shown to promote cell internalization of nanocarriers, maximizing the uptake of the (photo)therapeutic agents.[57]

RESULTS AND DISCUSSION

Synthesis and Characterization of GdSand. The synthesis of the GdSand was performed in a similar manner to previous syntheses by a base-promoted cyclization of 6-*tert*-butylnaphthalo-2,3-dinitrile with 1,8-diazabicycloundec-7-ene (DBU) and the rare-earth metal salt $Gd(OAc)_3 \cdot 4H_2O$.[39] As previously observed with lanthanide bis(macrocyclic) complexes, oxidation of the anionic sandwich complex (blue) to the stable neutral complex (green) occurred, due to the formation of a radical cation on one of the naphthalocyanine rings.[39,58,59] Purification was performed by silica gel chromatography

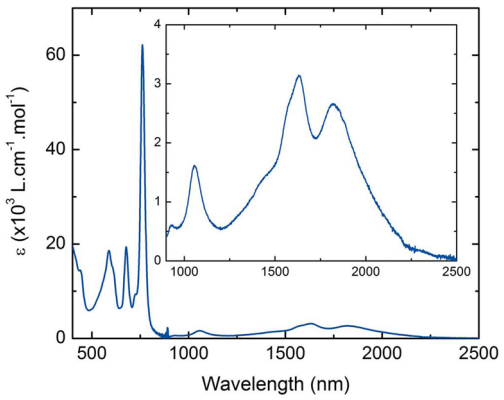

Figure 3. UV−vis−NIR absorption spectrum of GdSand in CCl_4 ([GdSand] = 1.28 × 10^{-5} M).

and size-exclusion chromatography (Sephadex LH-20). The presence of the desired complex was confirmed by mass spectrometry (Figure S1), and the UV−vis−NIR absorption spectrum (Figure 3) of GdSand matched well with the reported data.[39] The peaks in the spectrum experienced a slight blue shift compared to previously reported values due to the low polarity of the IR-inactive solvent CCl_4, required to obtain a complete UV−vis−NIR absorption spectrum.

The absorption spectrum of GdSand afforded absorbance peaks in the visible region at 438, 596, and 677 nm. Absorbance in the infrared region occurred at 761 (Q-band), 1057, 1645, and 1854 nm. The absorbance maximum at 761 nm originates from the characteristic Q-band absorption of the naphthalocyanine ring fortuitously placed within the therapeutic window and possessed a high (6.0 × 10^4 L cm^{-1} mol^{-1}) molar absorption coefficient. Of significant importance to the hypothesis proposed in this investigation is the lowest energy absorption, with an absorbance at 1854 nm and absorption onset close to 2500 nm. This absorption originates from the intramolecular charge transfer between the two macrocycles, one of which is oxidized within the overall neutral complex.[39,58,59] It is the presence of the radical cation, shared across the macrocycles within the GdSand molecule, that gives rise to this exceptionally low energy absorption beyond that of the intense Q-band absorption in the NIR from the naphthalocyanine ring. Furthermore, the energy of this absorption suggested that lanthanide sandwich complexes possessing these low-energy absorptions should exclusively exhibit photothermal properties (*i.e.*, insufficient energy level to sensitize ground-state $^3O_2$) upon the absorption of light.

Formulation and Characterization of GdSand@cpHDL. Cell-penetrating high-density lipoprotein (cpHDL) was utilized to solubilize GdSand, as the dye was not soluble in aqueous solvents. The cpHDL was formed using minor modifications to an established procedure, using 175 molar equiv of 1-palmitoyl-2-oleoyl-*sn*-glycero-3-phosphocholine (POPC) to the TAT peptide-fused protein

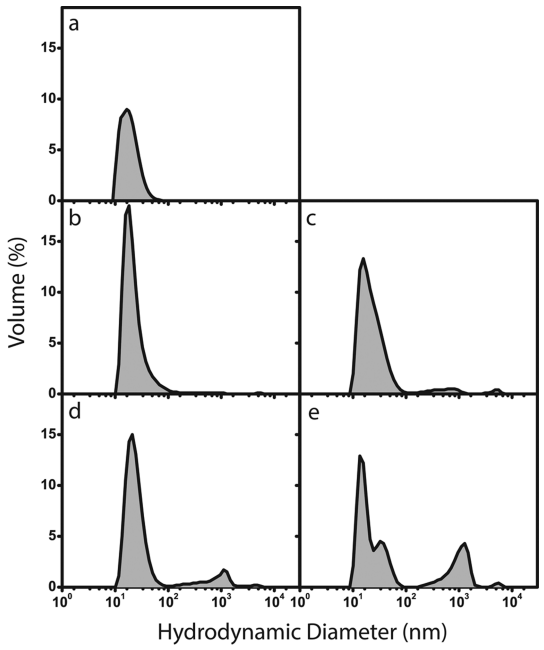

Figure 4. Size distribution of GdSand@cpHDL upon increasing GdSand stock concentration. [GdSand] = (a) 0 mM, (b) 0.12 mM, (c) 0.25 mM, (d) 0.49 mM, (e) 0.98 mM.

ApoA-1, which has the N-terminal 43 amino acid deleted.[57,60] Characterization of cpHDL by dynamic light scattering (DLS) measurement gave a mean diameter of 19 nm (Figure 4a). Formulation of GdSand@cpHDL was performed utilizing a previously reported protocol.[61] GdSand in DMSO (0.12−0.98 mM) was added to cpHDL in phosphate-buffered saline (PBS) (100 μg protein mL^{-1}), then incubated for 1 h at 37 °C. The corresponding GdSand@cpHDL was purified through a NAP-5 column to remove excess unencapsulated GdSand. The combination of the two chromatographic purifications of GdSand and the NAP-5 purification of GdSand@cpHDL affords little opportunity for any free Gd^{3+} to infiltrate the formulation. When the concentration of the GdSand stock solution was increased to 0.98 mM (39 μM in the reaction mixture), the resulting GdSand@cpHDL was found to contain a significant amount of large particles of more than 100 nm in diameter (Figure 4e), rendering corresponding DDS useless to exploit the EPR effect. On the other hand, GdSand@cpHDL prepared by using a 0.49 mM stock solution of GdSand (Figure 4d) maintained a uniform size (~90% of the total volume within the nanocarriers possess a mean diameter of 19 nm).

Complementary analysis of the size of this particular GdSand@cpHDL formulation (employing a 0.49 mM stock solution) was performed by mica flake electron microscopy (EM).[62,63] Utilizing this method the mean diameter of the GdSand@cpHDL was found to be ~31 ± 4 nm (Figure S2). The mean diameter of the GdSand@cpHDL particles was found to be slightly higher than the value obtained from DLS analysis, presumably arising from processing of the sample for the EM experiment. Regardless, the relative size distribution and the relative size are concurrent with the data from DLS analysis. In addition, GdSand@cpHDL was found to have a discoidal shape akin to the empty cpHDL nanocarrier, as well as the previously reported cpHDL loaded with porphyrin−fullerene conjugates.[63]

TABLE 1. Uptake of GdSand into cpHDL as a Function of Stock Solution (44 μg TAT peptide-fused protein mL^{-1})

GdSand stock (mM)	100% uptake (μmol)	obsd uptake (μmol)	dye uptake (%)	GdSand/protein (μmol g^{-1})
0.12	1.97×10^{-3}	3.68×10^{-4}	19	8
0.25	3.94×10^{-3}	6.01×10^{-4}	15	14
0.49	7.88×10^{-3}	7.92×10^{-4}	10	18

The GdSand@cpHDL particles were characterized by UV−vis−NIR spectrophotometry (Figure S3), showing a red-shift in the Q-band maximum observed at 761 nm in CCl_4 to 766 nm when encapsulated in the nanocarrier in saline solution. Presumably the red-shift originates from the polarity-induced aggregation phenomena experienced by the GdSand when moving from the nonpolar solvent CCl_4 to the POPC core of the cpHDL nanocarrier.

The uptake of GdSand into the cpHDL nanocarrier was determined by lyophilizing aliquots of GdSand@cpHDL prior to dissolving in methyl oleate and measurement by UV−vis−NIR spectrophotometry (Figure S4). Methyl oleate was employed as the solvent for the measurement, as it allowed the acquisition of GdSand spectra consistent with that from GdSand@cpHDL in saline as a result of its lipidic composition (comparable to the POPC of cpHDL), although the Q-band absorption maximum was slightly blue-shifted to 763 nm (Figure S5). The uptake of GdSand into cpHDL was calculated for the formulations that provided a suitably uniform DLS profile (0.12−0.49 mM GdSand stock). The uptake was quite low (10−19%), consistent with the observation of unencapsulated dye, retained at the top of the NAP-5 column during purification (data not shown). In spite of this, the amount of GdSand taken up (*i.e.*, GdSand/protein) by the cpHDL increased with increasing concentration of GdSand in the stock solution (Table 1). The uptake of the GdSand@cpHDL utilizing the 0.98 mM GdSand stock was not assessed due to its unsuitable DLS size profile (Figure 4e). Therefore, the formulations prepared by using 0.49 mM GdSand (0.79 μM GdSand in final mixture) were subjected to further investigation.

Photothermal Ability of GdSand@cpHDL with Increasing Laser Power. Assessment of the photothermal ability of GdSand@cpHDL as a function of laser power was determined by using an aliquot of solution (500 μL, OD_{770} = 0.10, 0.33 μM GdSand) prewarmed at 37 °C for 5 min prior to irradiation with a NIR laser (770 nm, 1500 mW, 20 min, Figure 5). All the solutions exhibited a constant photothermal response as a function of laser power across the 20 min irradiation time. Furthermore, plotting the temperature increase of the solution

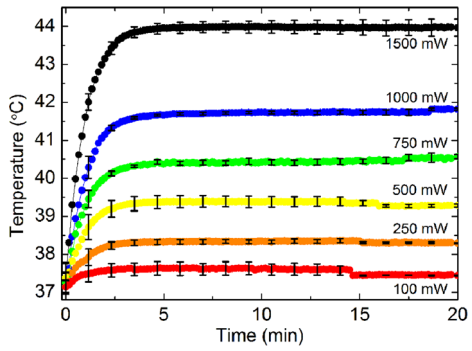

Figure 5. PTT ability of GdSand@cpHDL as a function of laser power (OD_{770} = 0.1, 0.33 μM GdSand λ_{ex} = 770 nm, 20 min), performed in triplicate.

at t = 10 min demonstrates a linear response with the incident laser power (Figure S6). This demonstrated that the photothermal dose administered to the system could be controlled through regulation of the incident laser power.

Comparison of Photothermal Ability between GdSand and Indocyanine Green (ICG). ICG is a dye with an absorption at 800 nm utilized as an NIR clinical imaging agent.[64−66] This unique absorption property has led to the use of ICG as a molecular light-absorbing component in several photothermal therapeutic formulations.[26−30] Therefore, we decided to compare the photothermal properties of the ICG-incorporated cpHDL (ICG@cpHDL) with GdSand@cpHDL. ICG@cpHDL was successfully prepared in a similar manner to that for GdSand, and the result of the experiment is given in Figure 6a. The saline blank recorded an increase of 1.8 °C to a final temperature of 38.8 °C when using a laser power of 1500 mW. Under this condition, the temperature of the GdSand@cpHDL solution had a quick rising phase followed by a sustained plateau at 44.4 °C. In contrast, the solution of ICG@cpHDL managed a maximum temperature of 43.4 °C after ~3 min of irradiation, prior to the gradual decrease in the temperature of the solution. This result demonstrated the improved photostability of GdSand compared to ICG, as decomposition of the cyanine dye[67−69] precluded it from maintaining an elevated temperature (*vide infra*).

The relative photothermal stabilities of GdSand and ICG were further investigated by the acquisition of UV−vis−NIR absorption spectra before and after irradiation with laser light. The result, shown in Figure 6b, revealed that GdSand@cpHDL demonstrated a 54% decrease in absorption at 770 nm, while ICG@cpHDL experienced full decomposition of the dye. This observation is consistent with differences in photothermal efficiency of the two dyes, where the ICG within the ICG@cpHDL experienced photodecomposition, resulting in an inability to maintain elevated temperature upon irradiation. The improved photothermal stability of GdSand is an essential feature for application in photothermal therapy *via* a mild hyperthermic

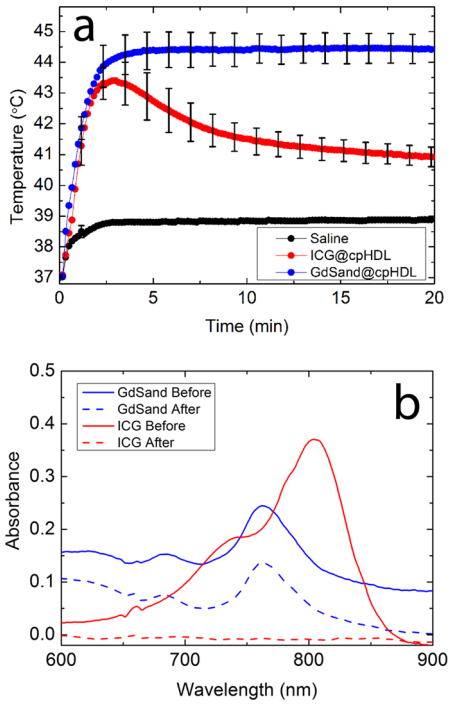

Figure 6. (a) Photothermal activity (λ_{ex} = 770 nm, 1500 mW, 20 min) of optically matched (OD_{770} = 0.24, 0.79 μM GdSand) solutions of GdSand@cpHDL (blue) and ICG@cpHDL (red) and saline (black), performed in triplicate. (b) UV−vis−NIR absorption spectra of GdSand@cpHDL (blue) and ICG@cpHDL (red) solutions before and after irradiation with laser light (OD_{770} = 0.24, 0.79 μM GdSand, λ_{ex} = 770 nm, 1500 mW, 20 min).

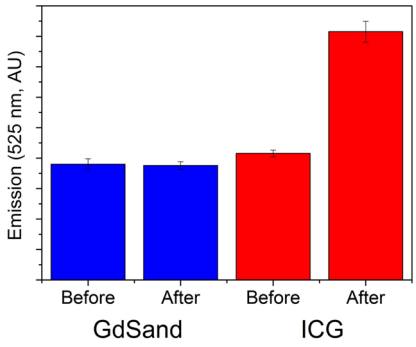

Figure 7. Singlet oxygen detection using SOSGR of GdSand@cpHDL and ICG@cpHDL before and after irradiation (λ_{ex} = 770 nm, 1500 mW, 20 min). Experiments were performed in triplicate. Error bars represent standard error.

pathway, as prolonged elevated temperatures are required (*vide supra*).

The prediction of an exclusively photothermal mode of action for GdSand@cpHDL was investigated by using the singlet oxygen sensor green reagent (SOSGR, Invitrogen). SOSGR exclusively reacts with $^1O_2$ in the event of its generation, resulting in an enhancement of fluorescence intensity (Figure 7). This experiment revealed that although ICG@cpHDL does indeed exhibit photothermal abilities, the photoresponsiveness of this molecule cannot be ascribed to solely PTT or PDT action, but rather a combination of

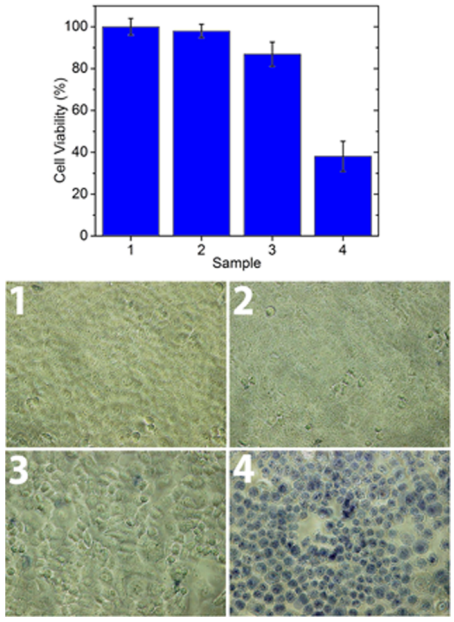

Figure 8. Cell viability column graph (top) and micrographs of trypan blue stained NCI-H460 cells (bottom). Sample number: (1) −inc/−irr, (2) −inc/+irr, (3) +inc/−irr, (4) +inc/+irr, where the symbol (−/+) indicates the use of incubation (inc) and/or irradiation (irr) treatment. Experiments were performed in triplicate. Error bars represent the standard error.

both, and the rapid decomposition of ICG would result from the latter action. Conversely, illumination of GdSand@cpHDL did not yield an appreciable amount of $^1O_2$, indicating that the mode of action of GdSand@cpHDL is purely photothermal, and the rationale for exclusive photothermal behavior is valid (*vide supra*).

Further investigation of the photostability of the two formulations was performed by conducting a densitometric analysis, to determine the integrity of the protein moiety within cpHDL after irradiation (Figure S7). Densitometric analysis revealed that 78% of the protein in the GdSand@cpHDL is intact after the irradiation period, and ICG@cpHDL experiences a slightly higher degree of nanocarrier destruction of the protein after laser exposure, with 68% of the peptide intact after laser irradiation. This result is consistent with the enhanced photostability of the GdSand@cpHDL observed from PTT, UV−vis−NIR, and SOSGR experiments.

***In Vitro* Photokilling of Human Cancer Cells by GdSand@cpHDL.** NCI-H460 human lung cancer cells were treated with GdSand@cpHDL in the presence of serum. After an incubation time of 24 h (time required for sufficient cell internalization of the DDS) the cells were quickly washed with the growth medium and then irradiated (770 nm, 1500 mW, 20 min). Then, cell viabilities were assessed by means of a colorimetric assay. The control experiment, where untreated cells were only irradiated (Figure 8, sample 2), gave a cell viability of 98%. When the cells were incubated with GdSand@cpHDL and not irradiated (Figure 8, sample 3), a cell viability of 87% was observed. These results show that the GdSand@cpHDL does not drastically affect cell viability (*i.e.*, nontoxic). Although we have purified the GdSand by silica gel and Sephadex chromatography and the GdSand@cpHDL by a NAP-5 column to remove any free gadolinium, the small decrease in cell viability could be a result of a slight *in vitro* toxicity of GdSand. Upon irradiation of the cells treated with GdSand@cpHDL (Figure 8, sample 4), a striking reduction in cell viability (38%) was observed, demonstrating selective photothermal destruction of the cells. In fact, the temperature of the GdSand@cpHDL-containing growth medium in the same cell culture system was increased to a similar level to the result shown in Figures 5 and 6 (data not shown).

The presence of GdSand within the cells after incubation was confirmed by its extraction from the cell lysate (Figure S8). The resulting absorption spectrum confirmed the presence of GdSand in the lysate also enabled calculation of a GdSand@cpHDL uptake of 45% by comparing the ratio of absorbance at 770 nm with the GdSand@cpHDL-containing growth medium (OD_{770} = 0.24) used in the cell experiment.

To further support the observations from the colorimetric assay, the cells were stained with trypan blue to confirm the presence of dead cells. The use of trypan blue is commonly used to assay cell viability in photothermal therapeutic studies.[13,16,20,23,29] After washing the cells and replacement of the growth medium containing trypan blue, a clear contrast before and after irradiation (Figure 8, samples 3 and 4) could be differentiated upon recording the bright field images of the cells.

CONCLUSIONS

The gadolinium-containing bisnapthalocyanine sandwich complex (GdSand) was successfully encapsulated into a nanocarrier cpHDL, functionalized with a cell-penetrating TAT peptide, for the first time. The nanocarrier enabled cell internalization of GdSand after 24 h of incubation. GdSand@cpHDL exhibited photothermal heat generation properties, demonstrating the ability to sustain an elevated temperature above 44 °C upon the absorption of NIR laser light. Furthermore, it was established that GdSand@cpHDL exclusively generates heat upon light absorption, with no $^1O_2$ detected, whereas ICG@cpHDL concomitantly generated heat and $^1O_2$, which inactivated the formula itself. GdSand@cpHDL decreased the cell viability of human cancer cells in a NIR-irradiation-dependent manner. Having demonstrated the proof-of-principle ability of the lanthanide sandwich complex to exhibit exclusive photothermal response and successful application as a photothermal therapeutic, we intend to explore the synthesis of second-generation lanthanide

sandwich complexes with improved solubility in cpHDL, improved photothermal stability, aqueous solubility, and secondary functionalization with elements to promote cellular recognition.

METHODS

Reagents. All chemicals were purchased from Sigma Aldrich, Wako Chemicals, or TCI Japan. NCI-H460 human lung cancer cells were from the National Cancer Institute (Frederick, MD, USA) and maintained in a growth medium of phenol red-free RPM 1640 supplemented with 5% FBS, 100 μg mL^{-1} penicillin, and 100 μg mL^{-1} streptomycin. The cells were cultured in 5% CO_2 and 95% air and were passaged every 3−4 days. The synthesis of GdSand was performed using the previously reported procedure.[39] The TAT peptide-fused protein ApoA-1, which has the N-terminal 43 amino acid deleted, was expressed in *E. coli* and purified according to the established method.[50]

Formulation of cpHDL. The procedure reported by Rogers *et al.* was used with minor modifications.[60] POPC was solubilized in PBS containing 30 mg mL^{-1} sodium cholate. The TAT peptide-fused protein ApoA-1 in 4 M urea PBS and POPC solutions were mixed at a 175:1 molar ratio of POPC to protein. The mixture was incubated overnight at room temperature, then dialyzed against PBS at 4 °C using a Spectra/Por dialysis membrane (MWCO 50 000). The reconstituted cpHDL solution was centrifuged at 16500*g* at 4 °C for 10 min to remove any debris.

Formulation of GdSand@cpHDL and ICG@cpHDL. Using a predetermined protocol,[61] a DMSO solution of dye (16 μL, 0.12−0.98 mM) was added to a PBS solution of cpHDL (400 μL, 100 μg mL^{-1}), and the mixture was incubated at 37 °C for 1 h. The GdSand@cpHDL formed was purified with a NAP-5 column (GE Healthcare UK Ltd., Buckinghamshire, England) equilibrated with saline. ICG@cpHDL was prepared in an analogous fashion prior to dilution in order to match the OD_{770} of GdSand@cpHDL solution in the comparison experiment. Diameters of dye-loaded HDLs were measured with a ZetaSizer Nano Z (Malvern, Worcestershire, UK).

UV−Vis−NIR Spectrophotometry. This was measured with a Cary 5 (Varian, Melbourne, Australia) or a UV-1600 (Shimadzu, Kyoto, Japan) UV−vis−NIR spectrophotometer.

Determination of GdSand Incorporation in GdSand@cpHDL. A calibration curve was made by acquiring UV−vis−NIR absorption spectra of stock solutions of GdSand in methyl oleate (Figure S3). Using the absorbance of GdSand at λ_{max} = 773 nm, an extinction coefficient of 3×10^5 L cm^{-1} mol^{-1} was calculated, much greater than the 6×10^4 L cm^{-1} mol^{-1} obtained in CCl_4 presented in Figure 3. To quantify GdSand in cpHDL, aqueous samples of GdSand@cpHDL (prepared utilizing 0.12, 0.25, and 0.49 mM stock solutions of GdSand in DMSO) in saline were lyophilized, and GdSand was extracted with methyl oleate for acquisition of the UV−vis−NIR absorption spectrum. The absorbance was related back to the amount of GdSand in solution, giving the incorporation amount.

Mica Flake Electron Microscopy. The experiment was performed utilizing a previously reported method.[62,63] A suspension of finely ground mica flakes (2 drops) was added to a solution of GdSand@cpHDL (500 μL, OD = 0.24, 0.79 μM GdSand, 44 μg mL^{-1} TAT-fused cpHDL). After a period of ∼30 s at 4 °C (to allow adsorption to the mica) the mica flakes were pelleted by centrifugation (∼500 rpm) and washed with KHMgE buffer (2×, 30 mM HEPES, 70 mM KCl, pH 7.2 plus 5 mM $MgCl_2$, 3 mM EGTA). The resulting pellet was positioned on a thin slice of chemically fixed rabbit lung. Rapid freezing of the corresponding sample was accomplished by abruptly applying the slurry of mica flakes onto a pure copper block, cooled in liquid He (Variant Instruments, USA). Freeze-fracturing of the frozen mica flake slurry was performed in a freeze-fracture system (EM-19500 JFDII, JEOL, Japan), followed by immediate etching at −104 °C for 4 min. The sample was rotary-shadowed with platinum at an angle of 11° to the surface and with carbon from the top. Separation of the replica was achieved by dissolving the mica by an overnight floatation with a solution of ∼10% $HF_{(aq)}$, prior to cleaning with 50% $HClO_{4(aq)}$, and washing with water (×3). The platinum replica was taken up onto an EM grid (Forvar-coated 200-mesh, copper, hexagonal, thin bar grid, GuilderGrids Co., UK). A detergent (Photo-Flo 600, Kodak) was utilized in all solutions that came into contact with the platinum replicas. The platinum replica was observed in a JEOL-JEM1400 (120 kV). For the stereo anaglyph, the stereopair images were obtained utilizing a ±10° tilt and a eucentric side-entry goniometer stage. The corresponding micrograph was analyzed using the ImageJ software[70,71] (version 1.47) to create a histogram in order to assess the size distribution of GdSand@cpHDL.

Photothermal Experiments. All experiments were performed in triplicate. For solution studies of photothermal ability, 500 μL aliquots of solutions were set in a microtube and placed in an incubator set at 37 °C, and the temperature was monitored with a fiber optic temperature sensor (Reflex, NEOPTIX) until equilibration was achieved (∼5 min). The fiber tip was arranged outside the laser spot. The solution was irradiated with a pulsed laser (Chameleon-RF femtosecond laser, Coherent, beam diameter 5 mm, 100−1500 mW) at 770 nm. Irradiation of NCI-H460 cells was achieved by placing the cell well on the incubator at 37 °C for 10 min prior to irradiation (770 nm, 1500 mW, 20 min).

Singlet Oxygen Detection Using SOSGR. Solutions of GdSand@cpHDL and ICG@cpHDL (OD_{770} = 0.24) were combined with singlet oxygen sensor green reagent (Invitrogen, 6 μM in DMSO), and the corresponding solution was subjected to irradiation by laser light (770 nm, 1500 mW, 20 min). The reaction product of SOSGR excited at 475 nm and the fluorescence at 525 nm was measured after 50 times dilution.

Photothermal Killing of Cancer Cells. A concentrated solution of GdSand@cpHDL was prepared using an Amicon Ultra ultrafiltration device (100 kDa MWCO). The concentrated GdSand@cpHDL was diluted with growth medium (final OD_{770} = 0.24) and added to NCI-H460 cells (1×10^4 cells per well, 96-well plate) prior to incubation for 24 h. After this time, the wells were washed with fresh growth medium and irradiated immediately (770 nm, 1500 mW, 20 min) on a heating block at 37 °C. Cell viability was assessed using the Cell Counting Kit-8 and a model 550 microplate reader (Biorad Laboratories Inc.) following manufacturer protocols. The viability of the cells was deduced by using the difference between the optical density at 450 and 620 nm. All measurements were performed in triplicate. Dead cells were stained with trypan blue for 10 min. Phase contrast images of the cells were taken with a Biozero BZ-8000 (Keyence, Osaka, Japan).

Extraction of GdSand from Cells. GdSand@cpHDL (OD_{770} = 0.24) was added to NCI-H460 cells (1×10^4 cells per well, 96-well plate) prior to incubation for 24 h (37 °C, 5% CO_2, 95% air). After this time, the cells were washed twice with growth medium, scraped out, and lyophilized. Methyl oleate was added prior to sonication for 10 min, centrifugation, and analysis of the supernatant by UV−vis−NIR spectrophotometry.

Conflict of Interest: The authors declare no competing financial interest.

Supporting Information Available: High-resolution mass spectrum of GdSand (Figure S1); mica-flake EM micrograph (Figure S2) of GdSand@cpHDL; UV−vis−NIR absorption spectrum of GdSand@cpHDL in saline (Figure S3); calibration curve for ε of GdSand in methyl oleate (Figure S4); normalized UV−vis−NIR absorption spectra of GdSand in DMSO and methyl oleate with comparison to GdSand@cpHDL in saline (Figure S5); photothermal efficiency of GdSand@cpHDL as a function of incident laser power (Figure S6); densitometric analysis of TAT peptide-fused protein from GdSand@cpHDL and ICG@cpHDL before and after irradiation (Figure S7); absorption spectrum of GdSand@cpHDL from cell lysate (Figure S8). This material is available free of charge *via* the Internet at http://pubs.acs.org.

Acknowledgment. S.M. gratefully acknowledges the Japanese Society for the Promotion of Science (JSPS) for the award of a JSPS Postdoctoral Fellowship for Foreign Researchers.

REFERENCES AND NOTES

1. Jain, P. K.; Huang, X.; El-Sayed, I. H.; El-Sayed, M. A. Noble Metals on the Nanoscale: Optical and Photothermal Properties and Some Applications in Imaging, Sensing, Biology, and Medicine. *Acc. Chem. Res.* **2008**, *41*, 1578–1586.
2. Anderson, R. R.; Parrish, J. A. Selective Photothermolysis: Precise Micro-Surgery by Selective Absorption of Pulsed Radiation. *Science* **1983**, *220*, 524–527.
3. Matsumura, Y.; Maeda, H. A New Concept for Macromolecular Therapeutics in Cancer Chemotherapy: Mechanism of Tumoritropic Accumulation of Proteins and the Antitumor Agent Smancs. *Cancer Res.* **1986**, *46*, 6387–6392.
4. Krawczyk, P. M.; Eppink, B.; Essers, J.; Stap, J.; Rodermond, H.; Odijk, H.; Zelensky, A.; van Bree, C.; Stalpers, L. J.; Buist, M. R.; *et al*. Mild Hyperthermia Inhibits Homologous Recombination, Induces BRCA2 Degradation, and Sensitizes Cancer Cells to Poly (ADP-ribose) Polymerase-1 Inhibition. *Proc. Natl. Acad. Sci. U.S.A.* **2011**, *108*, 9851–9856.
5. Brunetaud, J. M.; Mordon, S.; Maunoury, V.; Beacco, C. Non-PDT Uses of Lasers in Oncology. *Lasers Med. Sci* **1995**, *10*, 3–8.
6. Lanigan, S. Therapeutic Applications: Dermatology-Selective Photothermolysis. In *Handbook of Laser Technology and Applications*; Jones, J. D. C.; Webb, C. E., Eds.; Taylor & Francis: New York, 2003; pp 2045−2053.
7. Dewey, W. C. Arrhenius Relationships from the Molecule and Cell to the Clinic. *Int. J. Hyperthermia* **1994**, *10*, 457–483.
8. Svaasand, L. O.; Gomer, C. J.; Morinelli, E. A. On the Physical Rationale of Laser Induced Hyperthermia. *Lasers Med. Sci.* **1990**, *5*, 121–128.
9. Chen, W. R.; Adams, R. L.; Bartels, K. E.; Nordquist, R. E. Chromophore-Enhanced in-Vivo Tumor-Cell Destruction Using an 808-nm Diode-Laser. *Cancer Lett.* **1995**, *94*, 125–131.
10. Borrelli, M. J.; Wong, R. S. L.; Dewey, W. C. A Direct Correlation between Hyperthermia-Induced Membrane Blebbing and Survival in Synchronous G1 Cho Cells. *J. Cell. Physiol.* **1986**, *126*, 181–190.
11. Kowal-Vern, A.; McGill, V.; Walenga, J. M.; Gamelli, R. L. Antithrombin III Concentrate in the Acute Phase of Thermal Injury. *Burns* **2000**, *26*, 97–101.
12. Parrish, J. A. New Concepts in Therapeutic Photomedicine; Photochemistry, Optical Targeting and the Therapeutic Window. *J. Invest. Dermatol.* **1981**, *77*, 45–50.
13. Jelveh, S.; Chithrani, D. B. Gold Nanostructures as a Platform for Combinational Therapy in Future Cancer Therapeutics. *Cancers* **2011**, *3*, 1081–1110.
14. Huang, X.; Jain, P. K.; El-Sayed, I. H.; El-Sayed, M. A. Plasmonic Photothermal Therapy (PPTT) Using Gold Nanoparticles. *Lasers Med. Sci.* **2008**, *23*, 217–228.
15. Hu, M.; Chen, J.; Li, Z. Y.; Au, L.; Hartland, G. V.; Li, X.; Marquez, M.; Xia, Y. Gold Nanostructures: Engineering Their Plasmonic Properties for Biomedical Applications. *Chem. Soc. Rev.* **2006**, *35*, 1084–1094.
16. Huang, X.; El-Sayed, I. H.; Qian, W.; El-Sayed, M. A. Cancer Cell Imaging and Photothermal Therapy in the Near-Infrared Region by Using Gold Nanorods. *J. Am. Chem. Soc.* **2006**, *128*, 2115–2120.
17. Chen, J.; Wang, D.; Xi, J.; Au, L.; Siekkinen, A.; Warsen, A.; Li, Z. Y.; Zhang, H.; Xia, Y.; Li, X. Immuno Gold Nanocages with Tailored Optical Properties for Targeted Photothermal Destruction of Cancer Cells. *Nano Lett.* **2007**, *7*, 1318–1322.
18. Cobley, C. M.; Chen, J.; Cho, E. C.; Wang, L. V.; Xia, Y. Gold Nanostructures: A Class of Multifunctional Materials for Biomedical Applications. *Chem. Soc. Rev.* **2011**, *40*, 44–56.
19. Lal, S.; Clare, S. E.; Halas, N. J. Nanoshell-Enabled Photothermal Cancer Therapy: Impending Clinical Impact. *Acc. Chem. Res.* **2008**, *41*, 1842–1851.
20. Kim, J.; Park, S.; Lee, J. E.; Jin, S. M.; Lee, J. H.; Lee, I. S.; Yang, I.; Kim, J. S.; Kim, S. K.; Cho, M. H.; *et al*. Designed Fabrication of Multifunctional Magnetic Gold Nanoshells and Their Application to Magnetic Resonance Imaging and Photothermal Therapy. *Angew. Chem., Int. Ed.* **2006**, *45*, 7754–7758.
21. Chen, J.; Glaus, C.; Laforest, R.; Zhang, Q.; Yang, M.; Gidding, M.; Welch, M. J.; Xia, Y. Gold Nanocages as Photothermal Transducers for Cancer Treatment. *Small* **2010**, *6*, 811–817.
22. Huang, X.; El-Sayed, M. A. Gold Nanoparticles: Optical Properties and Implementations in Cancer Diagnosis and Photothermal Therapy. *J. Adv. Res.* **2010**, *1*, 13–28.
23. Nam, J.; Won, N.; Jin, H.; Chung, H.; Kim, S. pH-Induced Aggregation of Gold Nanoparticles for Photothermal Cancer Therapy. *J. Am. Chem. Soc.* **2009**, *131*, 13639–13645.
24. Au, L.; Zheng, D.; Zhou, F.; Li, Z. Y.; Li, X.; Xia, Y. A Quantitative Study on the Photothermal Effect of Immuno Gold Nanocages Targeted to Breast Cancer Cells. *ACS Nano* **2008**, *2*, 1645–1652.
25. Jin, Y.; Jia, C.; Huang, S. W.; O'Donnell, M.; Gao, X. Multifunctional Nanoparticles as Coupled Contrast Agents. *Nat. Commun.* **2010**, *1*, 41.
26. Zheng, X.; Xing, D.; Zhou, F.; Wu, B.; Chen, W. R. Indocyanine Green-Containing Nanostructure as Near Infrared Dual-Functional Targeting Probes for Optical Imaging and Photothermal Therapy. *Mol. Pharmaceutics* **2011**, *8*, 447–456.
27. Zheng, M.; Yue, C.; Ma, Y.; Gong, P.; Zhao, P.; Zheng, C.; Sheng, Z.; Zhang, P.; Wang, Z.; Cai, L. Single-Step Assembly of DOX/ICG Loaded Lipid-Polymer Nanoparticles for Highly Effective Chemo-Photothermal Combination Therapy. *ACS Nano* **2013**, *7*, 2056–2067.
28. Zheng, X.; Zhou, F.; Wu, B.; Chen, W. R.; Xing, D. Enhanced Tumor Treatment Using Biofunctional Indocyanine Green-containing Nanostructure by Intratumoral or Intravenous Injection. *Mol. Pharmaceutics* **2012**, *9*, 514–522.
29. Yu, J.; Javier, D.; Yaseen, M. A.; Nitin, N.; Richards-Kortum, R.; Anvari, B.; Wong, M. S. Self-Assembly Synthesis, Tumor Cell Targeting, and Photothermal Capabilities of Antibody-Coated Indocyanine Green Nanocapsules. *J. Am. Chem. Soc.* **2010**, *132*, 1929–1938.
30. Tang, Y.; McGoron, A. J. Combined Effects of Laser−ICG Photothermotherapy and Doxorubicin Chemotherapy on Ovarian Cancer Cells. *J. Photochem. Photobiol., B* **2009**, *97*, 138–144.
31. Zhou, F.; Wu, S.; Wu, B.; Chen, W. R.; Xing, D. Mitochondria-Targeting Single-Walled Carbon Nanotubes for Cancer Photothermal Therapy. *Small* **2011**, *7*, 2727–2735.
32. Krishna, V.; Stevens, N.; Koopman, B.; Moudgil, B. Optical Heating and Rapid Transformation of Functionalized Fullerenes. *Nat. Nanotechnol.* **2010**, *5*, 330–334.
33. Wu, M. C.; Deokar, A. R.; Liao, J. H.; Shih, P. Y.; Ling, Y. C. Graphene-Based Photothermal Agent for Rapid and Effective Killing of Bacteria. *ACS Nano* **2013**, *7*, 1281–1290.
34. Cheng, C.; Yang, K.; Chen, Q.; Liu, Z. Organic Stealth Nanoparticles for Highly Effective *in Vivo* Near-Infrared Photothermal Therapy of Cancer. *ACS Nano* **2012**, *6*, 5605–5613.
35. Ng, K. K.; Lovell, J. F.; Vedadi, A.; Hajian, T.; Zheng, G. Self-Assembled Porphyrin Nanodiscs with Structure-Dependent Activation for Phototherapy and Photodiagnostic Applications. *ACS Nano* **2013**, *7*, 3484–3490.
36. Jin, C. S.; Lovell, J. F.; Chen, J.; Zheng, G. Ablation of Hypoxic Tumors with Dose-Equivalent Photothermal, but Not Photodynamic, Therapy Using a Nanostructured Porphyrin Assembly. *ACS Nano* **2013**, *7*, 2541–2550.
37. Lovell, J. F.; Jin, C. S.; Huynh, E.; Jin, H.; Kim, C.; Rubinstein, J. L.; Chan, W. C. W.; Cao, W.; Wang, L. V.; Zheng, G. Porphysome Nanovesicles Generated by Porphyrin Bilayers for Use as Multimodal Biophotonic Contrast Agents. *Nat. Mater.* **2011**, *10*, 324–332.
38. Blanco, E.; Hsiao, A.; Mann, A. P.; Landry, M. G.; Meric-Bernstam, F.; Ferrari, M. Nanomedicine in Cancer Therapy: Innovative Trends and Prospects. *Cancer Sci.* **2011**, *102*, 1247–1252.
39. Jiang, J.; Liu, W.; Poon, K. W.; Du, D.; Arnold, D. P.; Ng, D. K. P. Synthesis, Spectroscopic, and Electrochemical Properties of Rare Earth Double-Deckers with Tetra(tert-butyl)-2,3-naphthalocyaninato Ligands. *Eur. J. Inorg. Chem.* **2000**, *2000*, 205–209.

40. Collins, G. C. S.; Schiffrin, D. J. The Electrochromic Properties of Lutetium and Other Phthalocyanines. *J. Electroanal. Chem.* **1982**, *139*, 335–369.
41. Komatsu, T.; Ohta, K.; Fujimoto, T.; Yamamoto, I. Chromic Materials. Part 1 - Liquid-Crystalline Behaviour and Electrochromism in Bis(octakis-*n*-alkylphthalocyaninato)lutetium-(III) Complexes. *J. Mater. Chem.* **1994**, *4*, 533–536.
42. Kirin, I. S.; Moskalev, P. N.; Makashev, Y. A. Formation of Unusual Phthalocyanines of the Rare-Earth Elements. *Russ. J. Inorg. Chem.* **1965**, *10*, 1065–1066.
43. Jiang, J.; Ng, D. K. P. A Decade Journey in the Chemistry of Sandwich-Type Tetrapyrrolato-Rare Earth Complexes. *Acc. Chem. Res.* **2009**, *42*, 79–88.
44. Brasseur, N.; Nguyen, T. L.; Langlois, R.; Ouellet, R.; Marengo, S.; Houde, D.; van Lier, J. E. Synthesis and Photodynamic Activities of Silicon 2,3-Naphthalocyanine Derivitives. *J. Med. Chem.* **1994**, *37*, 415–420.
45. Vollano, J. F.; Bossard, G. E.; Martellucci, S. A.; Darkes, M. C.; Abrams, M. J.; Brooks, R. C. The Synthesis and *in Vitro* Photodynamic Activity of a Series of Novel Ruthenium(II)-2,3-Naphthalocyanines. *J. Photochem. Photobiol., B* **1997**, *37*, 230–235.
46. Shopova, M.; Woehrle, D.; Mantareva, V.; Mueller, S. Naphthalocyanine Complexes as Potential Photosensitizers for Photodynamic Therapy of Tumors. *J. Biomed. Opt.* **1999**, *4*, 276–285.
47. Song, L.; Li, H.; Sunar, U.; Chen, J.; Corbin, I.; Yodh, A. G.; Zheng, G.; Naphthalocyanine–Reconstituted, L. D. L. Nanoparticles for *in Vivo* Cancer Imaging and Treatment. *Int. J. Nanomed.* **2007**, *2*, 767–774.
48. Luan, L.; Ding, L.; Zhang, W.; Shi, J.; Yu, X.; Liu, W. A Naphthalocyanine Based Near–Infrared Photosensitizer: Synthesis and *in Vitro* Photodynamic Activities. *Bioorg. Med. Chem. Lett.* **2013**, *23*, 3775–3779.
49. Ruben, S.; Perkins, A.; Purcell, R.; Joung, K.; Sia, R.; Burghoff, R.; Haseltine, W. A.; Rosen, C. A. Structural and Functional Characterization of Human Immunodeficiency Virus Tat Protein. *J. Virol.* **1989**, *63*, 1–8.
50. Vivès, E.; Brodin, P.; Lebleu, B. A Truncated HIV-1 Tat Protein Basic Domain Rapidly Translocates through the Plasma Membrane and Accumulates in the Cell Nucleus. *J. Biol. Chem.* **1997**, *272*, 16010–16017.
51. Frankel, A. D.; Pabo, C. O. Cellular Uptake of the Tat Protein from Human Immunodeficiency Virus. *Cell* **1988**, *55*, 1189–1193.
52. Brooks, H.; Lebleu, B.; Vivès, E. Tat Peptide-Mediated Cellular Delivery: Back to Basics. *Adv. Drug Delivery Rev.* **2005**, *57*, 559–577.
53. Kaplan, I. M.; Wadia, J. S.; Dowdy, S. F. Cationic TAT Peptide Transduction Domain Enters Cells by Macropinocytosis. *J. Controlled Release* **2005**, *102*, 247–253.
54. Fawell, S.; Seery, J.; Daikh, Y.; Moore, C.; Chen, L. L.; Pepinsky, B.; Barsoum, J. Tat-Mediated Delivery of Heterologous Proteins Into Cells. *Proc. Natl. Acad. Sci. U.S.A.* **1994**, *91*, 664–668.
55. Campbell, R. B.; Fukumura, D.; Brown, E. B.; Mazzola, L. M.; Izumi, Y.; Jain, R. K.; Torchilin, V. P.; Munn, L. L. Cationic Charge Determines the Distribution of Liposomes Between the Vascular and Extravascular Compartments of Tumors. *Cancer Res.* **2002**, *62*, 6831–6836.
56. Schmitt-Sody, M.; Strieth, S.; Krasnici, S.; Sauer, B.; Schulze, B.; Teifel, M.; Michaelis, U.; Naujoks, K.; Dellian, M. Neovascular Targeting Therapy: Paclitaxel Encapsulated in Cationic Liposomes Improves Antitumoral Efficacy. *Clin. Cancer Res.* **2003**, *9*, 2335–2341.
57. Murakami, T.; Wijagkanalan, W.; Hashida, M.; Tsuchida, K. Intracellular Drug Delivery by Genetically Engineered High Density Lipoprotein Nanoparticles. *Nanomedicine (London, U. K.)* **2010**, *5*, 867–879.
58. De Cian, A.; Moussavi, M.; Fischer, J.; Weiss, R. Synthesis, Structure, and Spectroscopic and Magnetic Properties of Lutetium(III) Phthalocyanine Derivatives: $LuPc_2.CH_2Cl_2$ and $[LuPc(OAc)(H_2O)_2]\cdot H_2O\cdot 2CH_3OH$. *Inorg. Chem.* **1985**, *24*, 3162–3167.
59. Markovitsi, D.; Tran-Thi, T. H.; Even, R.; Simon, J. Near Infrared Absorption Spectra of Lanthanide Bis-Phthalocyanines. *Chem. Phys. Lett.* **1987**, *137*, 107–112.
60. Rogers, D. P.; Brouillette, C. G.; Engler, J. A.; Tendian, S. W.; Roberts, L.; Mishra, V. K.; Anantharamaiah, G. M.; Lund-Katz, S.; Phillips, M. C.; Ray, M. J. Truncation of the Amino Terminus of Human Apolipoprotein A-I Substantially Alters Only the Lipid-Free Conformation. *Biochemistry* **1997**, *36*, 288–300.
61. Murakami, T.; Tsuchida, K.; Hashida, M.; Imahori, H. Size Control of Lipid Based Drug Carriers by Drug Loading. *Mol. BioSyst.* **2010**, *6*, 789–791.
62. Heuser, J. Protocol doe 3-D Visualization of Molecules on Mica *via* the Quick-Freeze, Deep-Etch Technique. *J. Electron Microsc. Tech.* **1989**, *13*, 244–263.
63. Numata, T.; Murakami, T.; Kawashima, F.; Morone, N.; Heuser, J. E.; Takano, Y.; Ohkubo, K.; Fukuzumi, S.; Mori, Y.; Imahori, H. Utilization of Photoinduced Charge–Separated State of Donor-Acceptor-Linked Molecules for Regulation of Cell Membrane Potential and Ion Transport. *J. Am. Chem. Soc.* **2012**, *134*, 6092–6095.
64. Sakka, S. G. Assessing Liver Function. *Curr. Opin. Crit. Care* **2007**, *13*, 207–214.
65. Landsman, M. L.; Kwant, G.; Mook, G. A.; Zijlstra, W. G. Light-Absorbing Properties, Stability, and Spectral Stabilization of Indocyanine Green. *J. Appl. Physiol.* **1976**, *40*, 575–583.
66. Dzurinko, V. L.; Gurwood, A. S.; Price, J. R. Intravenous and Indocyanine Green Angiography. *Optometry* **2004**, *75*, 743–755.
67. Zhou, J. F.; Chin, M. P.; Schafer, S. A. Aggregation and Degradation of Indocyanine Green. *Proc. SPIE* **1994**, *2128*, 495–505.
68. Björnsson, O. G.; Murphy, R.; Chadwick, V. S.; Björnsson, S. Physiochemical Studies on Indocyanine Green: Molar Lineic Absorbance, pH Tolerance, Activation Energy and Rate of Decay in Various Solvents. *J. Clin. Chem. Clin. Biochem.* **1983**, *21*, 453–458.
69. Gathje, J.; Steuer, R. R.; Nicholes, K. R. Stability Studies on Indocyanine Green Dye. *J. Appl. Physiol.* **1970**, *29*, 181–185.
70. Abramoff, M. D.; Magalhaes, P. J.; Ram, S. J. Image Processing with ImageJ. *Biophotonics Int.* **2004**, *11*, 36–42.
71. Schneider, C. A.; Rasband, W. S.; Eliceiri, K. W. NIH Image to ImageJ: 25 Years of Image Analysis. *Nat. Methods* **2012**, *9*, 671–675.